Journal of Physics: Conference Series **2687** (2024) 072034 doi:10.1088/1742-6596/2687/7/072034

FAIR SIS100 accelerating RF system - Modeling and analysis of the coupled LLRF control loops

C J Wegmann[1], L Kronshorst[1], S Orth[1], K Groß[2], H Klingbeil[1,2], D E M Lens[2], J S Schmidt[2], A Stuhl[2] and B Zipfel[2]

[1] Technische Universität Darmstadt, Karolinenplatz 5, 64289 Darmstadt, Germany
[2] GSI Helmholtzzentrum für Schwerionenforschung GmbH, Planckstraße 1, 64291 Darmstadt, Germany

E-mail: julien.wegmann@tu-darmstadt.de

Abstract. The SIS100 heavy ion synchrotron as core part of the Facility for Antiproton and Ion Research (FAIR) will be equipped with 14 accelerating RF stations in the first stage of realization. Each RF station consists of a tunable ferrite-loaded cavity powered by a tetrode amplifier. Further key components are a solid-state pre-amplifier, a power supply unit, and dedicated Low-Level Radio Frequency (LLRF) feedforward and feedback systems to control amplitude and phase of the cavity gap voltage as well as the resonance frequency. Each cavity has to provide up to 20 kV peak gap voltage in the frequency range from 1.1 to 3.2 MHz. While all components of the system have been successfully tested in the factory acceptance tests and transferred to the FAIR storage, the First-of-Series (FoS) RF station is still persistently operated at GSI to gain experience. For further insight into the LLRF part, especially the stability of the control loops, the inter-coupling of the three local control loops was analyzed with methods from control theory based on simplified but realistic models, which have been developed based on extensive measurements and analysis of the systems' behavior. In this contribution, the modeling as well as the analysis of the coupling between the LLRF control loops are discussed and the results are presented in comparison with measurements on the FoS system.

1. Introduction

The 14 RF stations of the acceleration system of the new FAIR SIS100 heavy ion synchrotron provide in total up to 280 kV to the high intensity beams. Systematical models of such an RF station were developed in order to analyze the cross couplings of the control loops using closed-loop control theory. Due to this focus, the driver amplifier, the tetrode and the inductively biased, ferrite-loaded cavity itself were modeled as a combined parallel equivalent circuit with variable parameters in a first step (Fig. 1). Three parameter fields were filled with data by extensive measurements and data fitting. Firstly, a Simulink model including lookup tables for the elements depending on the operating point was created. The relevant dynamics of the LLRF modules were already known and added to the model of the RF station. Only the amplitude modulator (AM) and the generation of the bias current were remodeled to achieve the desired accuracy. The modeling is summarized in the first section of this paper. Beam-loading effects [1, 2, 3, 4] are beyond the focus of this paper and are not considered here, because they are handled by suitable set-values [5, 6] and, in addition, by impedance reduction measures [7]. The cavities used for FAIR have quality factors below 50 and different control system topology, so

that conventional beam-loading analysis results are not applicable. Furthermore, an analytical model for the FAIR LLRF system is for the first time derived and validated in this work. After the validation of the two models using dedicated records taken from the FoS system, the cross couplings between the three control loops acting on the accelerating gap voltage are analyzed, both indicating the theoretical limits of the controller setup and showing reliable operation of the present LLRF system at all operating points.

2. Modeling for Simulink

2.1. Cavity

All measurements to create and validate the models were taken at the FoS RF system described in [8, 9]. In the first step, the modeling process is based on an RLC parallel resonant circuit (Fig. 1) as the equivalent lumped-element circuit of cavity and amplifiers near resonance [10].

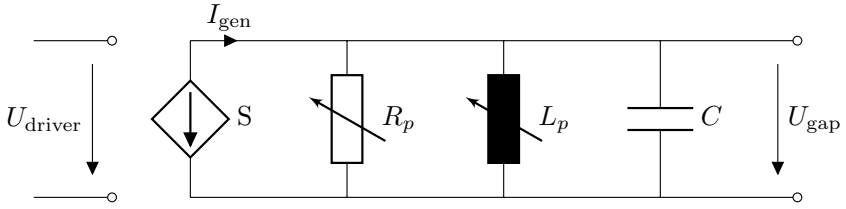

Figure 1. Lumped-element circuit of the RF system.

From the describing integro-differential equation

$$C\dot{V}_{\text{gap}}(t) + \frac{1}{R_{\text{p}}}V_{\text{gap}}(t) + \frac{1}{L_{\text{p}}}\int V_{\text{gap}}(t)\,\mathrm{d}t = SV_{\text{driver}}(t) \tag{1}$$

the transfer function

$$G(s) = \frac{V_{\text{gap}}(s)}{V_{\text{driver}}(s)} = \frac{\frac{S}{C}s}{s^2 + \frac{1}{CR_{\text{p}}}s + \frac{1}{CL_{\text{p}}}} \tag{2}$$

as a function of the complex Laplace variable s can be derived for fixed values of the parallel resistance R_{p}, parallel inductance L_{p} and transconductance S. In order to capture the tuning behavior of the cavity, at the very least L_{p} has to be adjustable via the biasing current I_{bias}. Therefore, values for the lumped-element parameters were experimentally determined from measurements of the FoS cavity system. Hereby, the value of the capacitance measured by the manufacturer of the cavity, $C = 310\,\text{pF}$, was assumed to be constant, while L_{p}, R_{p} and S were determined as parameter fields depending on both I_{bias} and the control voltage of the AM $V_{\text{AM,ctrl}}$. For every pair of values in $[I_{\text{bias}}, V_{\text{AM,ctrl}}]$ the system's input and output RF signals were recorded applying a slow, triangular frequency sweep to the input. A fit was used to extract frequency, gain, phase and offset, resulting in Bode plots of the system at the operating points. After extracting the maximum gain, resonance frequency and 3 dB-bandwidth, the values for L_{p}, R_{p} and S of the parallel resonant circuit's transfer function, Eq. (2) were calculated. The resulting three parameter fields were implemented in Simulink as lookup table blocks [11]. As an example, the high-resolution mapping of the parallel inductance $L_{\text{p}}(I_{\text{bias}}, V_{\text{AM,ctrl}})$ is shown in Fig. 2.

2.2. LLRF

The LLRF for control and synchronization is modularly built up by over 20 standardized analog and digital components mainly developed at GSI. An overview is given in [12, 13]. The LLRF

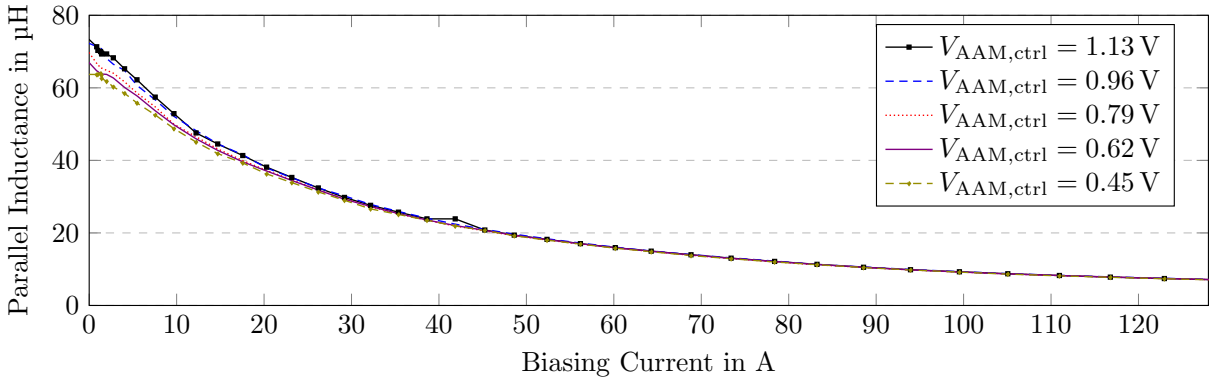

Figure 2. Identified parameter field of the inductance.

includes an interface to the central control system, but was set up locally for the presented work. A sketch of the cavity's local control system with its three main control loops is shown in Fig. 3. At the time of writing, the resonance and amplitude controller were implemented

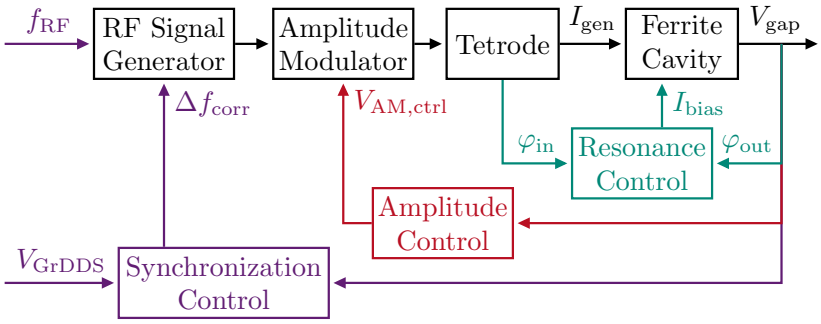

Figure 3. Simplified block diagram of the RF system.

as PI-controllers and the synchronization controller as a P-controller, configured such that the amplitude and synchronization control are significantly faster than the resonance control. During the analysis, the time behavior of the biasing was identified from measurements in open- and closed-loop operation and the amplitude modulator was individually measured to identify the amplitude gain as a function of the amplitude modulator control voltage $V_{\mathrm{AM,ctrl}}$ and the RF frequency.

3. Analytic modeling

In order to be able to utilize the general-purpose tools and methods from the theory of closed-loop control systems, an analytical model was generated. It is based on the same modeling approaches as the Simulink model, with the additional step of simplifying the behavior of each component into transfer functions. For the cavity itself, this was achieved again starting from Eq. (1) and by splitting RF signals into an amplitude and a phase signal, for example

$$V_{\mathrm{gap}}(t) = \hat{V}_{\mathrm{gap}}(t) \cdot \sin\left(\omega_{\mathrm{RF}} \cdot t + \varphi_{\mathrm{gap}}(t)\right) . \tag{3}$$

A linearization was performed and the resulting equations were simplified until Laplace transform could be applied. To account for the lumped-element parameters being identified

as parameter fields and therefore variable with time, they were handled as Taylor expansions during linearization, such as

$$L_{\mathrm{p}}(t) \approx L_{\mathrm{p,OP}} + \frac{\partial L_{\mathrm{p}}}{\partial I_{\mathrm{bias}}} \Delta I_{\mathrm{bias}}(t) + \frac{\partial L_{\mathrm{p}}}{\partial V_{\mathrm{AM,ctrl}}} \Delta V_{\mathrm{AM,ctrl}}(t)\,. \tag{4}$$

The respective operating point (OP) and derivative values were derived from the measured parameter fields. Figure 4 gives an overview of the resulting model. As an example, one matrix element is given in Eq. (5). With the matrices of transfer functions of the controllers $\mathbf{G}_{\mathrm{Ctrl}}(s)$ and of the sensors $\mathbf{G}_{\mathrm{Sens}}(s)$ being diagonal, the analytical model is a decentralized MIMO control system of dimension 3, i.e. the three individual control loops only interact due to cross couplings contained in the controlled system $\mathbf{G}_{\mathrm{Sys}}(s)$ [14]. The controlled variables are $\hat{V}_{\mathrm{gap}}$, φ_{sync} and φ_{imp} for amplitude, synchronization and resonance control respectively.

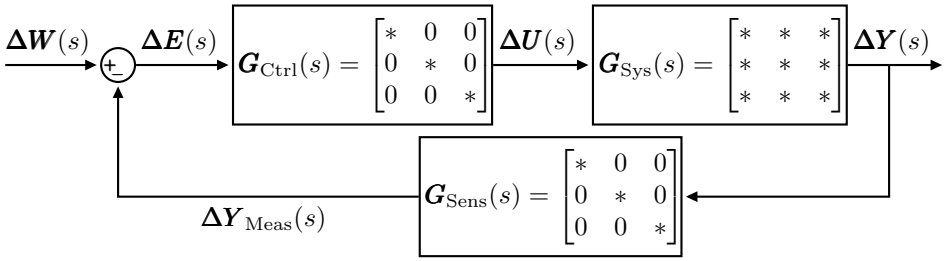

Figure 4. Overview of the analytical model in the topology of the standard control loop.

$$G_{\mathrm{Sys},33}(s) = \frac{4\pi \cdot \frac{\partial f_{\mathrm{res}}}{\partial I_{\mathrm{bias}}} \cdot \frac{\partial I_{\mathrm{bias}}}{\partial V_{\mathrm{bias,ctrl}}} \cdot \left[s^2\left(s+\frac{2}{\tau}\right) + (2\pi f_{\mathrm{RF}})^2 \cdot \left(2s+\frac{2}{\tau}\right)\right] + \frac{4\pi f_{\mathrm{RF}} \cdot \frac{\partial R_{\mathrm{p}}}{\partial I_{\mathrm{bias}}} \cdot \frac{\partial I_{\mathrm{bias}}}{\partial V_{\mathrm{bias,ctrl}}}}{R_{\mathrm{p}}\tau} \cdot \left[s\left(s+\frac{2}{\tau}\right) - s\left(2s+\frac{2}{\tau}\right)\right] + \frac{4\pi f_{\mathrm{RF}} \cdot \frac{\partial S}{\partial I_{\mathrm{bias}}} \cdot \frac{\partial I_{\mathrm{bias}}}{\partial V_{\mathrm{bias,ctrl}}}}{S\tau} \cdot \left[s\left(s+\frac{2}{\tau}\right) - s\left(2s+\frac{2}{\tau}\right)\right]}{\left[s^2\left(s+\frac{2}{\tau}\right)^2 + (2\pi f_{\mathrm{RF}})^2 \cdot \left(2s+\frac{2}{\tau}\right)^2\right] \cdot (T_{1,\mathrm{bias}}s+1) \cdot (T_{2,\mathrm{bias}}s+1)} \tag{5}$$

4. Model validation

The performance of the generated models was validated by recording the step response of all 9 transmission paths of the cavity control system and comparing the measurements with the respective predictions of the models. Figure 5 gives an example of how the impedance phase φ_{imp} is excited by the application of a reference step to the synchronization phase φ_{sync}.

In general, the models show a high level of accuracy in reproducing the behavior of the transmission paths. Specifically, the Simulink model manages to reproduce even fine details of the recorded signal shapes, as can be seen in the slight overshoot in the negative direction in Fig. 5. There exist two minor exceptions: the amplitude characteristic of tuning the cavity is not included in the analytical model due to linearization around the cavity being in resonance and the minor interactions between changes in the amplitude and the phase of the gap voltage are recreated inaccurately.

5. Analysis of coupled LLRF control loops

Due to the validation indicating that the generated models reproduce the main underlying physical behavior of the cavity system, the analysis of the control loops and their coupling was performed with the models, using coupling factors, relative gain array and Gershgorin bands for an analytical examination [14] underlined with simulations of the Simulink model in the time domain [15]. Because of its decentralized control structure, the closed-loop control system can be interpreted as containing three main transmission paths, from the three reference signals

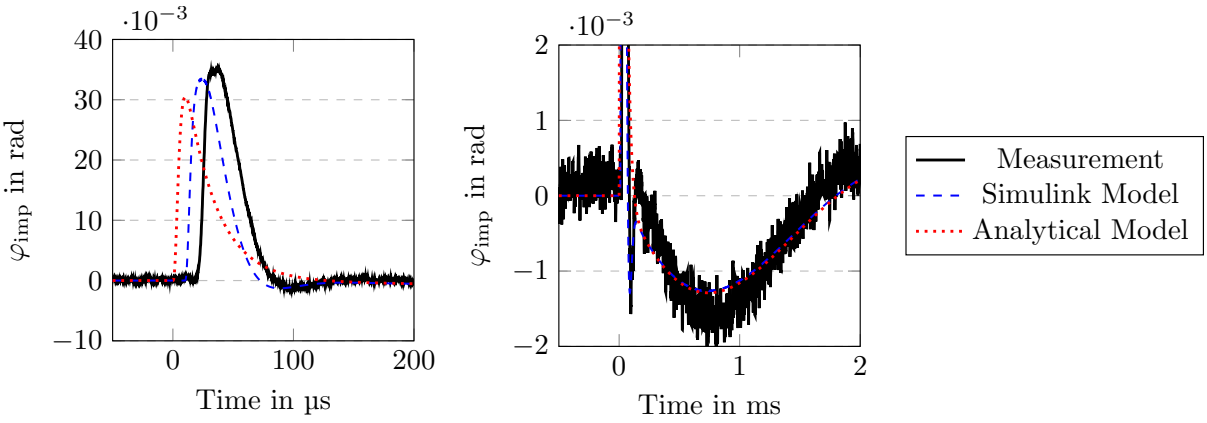

Figure 5. Excitation of φ_{imp} due to a reference step of 0.5 rad in $\varphi_{\mathrm{sync,ref}}$. Short- (left) and long-term behavior (right).

to their respective controlled variable, in addition to six cross coupling paths, connecting each reference signal with the controlled variables of the respective other two control loops. Hence, each activation of a single control loop creates a disturbance for the other two loops, exciting their controlled variables and thereby inducing a reaction from their controllers. Using the aforementioned tools, the extent and impact of these cross couplings is summarized in Table 1. Most prominently, every time the resonance control tunes the cavity, the amplitude and phase

Table 1. Extent and properties of the cross coupling.

		Activated Control Loop		
		Amplitude	Synchronization	Resonance Frequency
Disturbed Control Loop	Amplitude	Main Transmission Path	Minor Transient	Major Non-Transient
	Synchronization	Minor Transient	Main Transmission Path	Major Non-Transient
	Resonance Frequency	Minor Non-Transient	Minor Transient	Main Transmission Path

of the gap voltage experience a non-transient deviation of significant magnitude. Hence, a reaction of the other two control loops is always required in order to return amplitude and phase to their target value. In general, the faster amplitude and synchronization control are configured, the smaller the maximum occurring deviation can be kept. This at the same time also increases the disturbances arising in the impedance phase due to activation of these two control loops. However, since these disturbances are both less prominent and transient, the resulting impact on the resonance frequency is small. Since under normal circumstances no strong feedback between any two control loops can exist, the couplings between the control loops do not endanger the stability of the cavity system. The deduced relations were verified to

also hold for the detuned cavity [15, C. 4.2] e.g. due to beam-loading. Therefore, the currently chosen controller configuration addresses the existing couplings well and there is no indication that further countermeasures such as a feed-forward compensation of the resonance control's cross couplings are required.

6. Conclusion

The models derived from measurements of the FoS RF accelerating system reproduce the system's behavior accurately both in open- and closed-loop operation. The high-resolution mapping covers the majority of the system's operating range in frequency and voltage level. The analysis led to a deeper understanding of the underlying effects but also showed that present layout and configuration of the local control loops ensure stable operation within the future FAIR facility. The resonance control has a major influence on the amplitude and the synchronization phase, and therefore has to be and is set up to react slower than the other two control loops. Thereby the speed of the control loops is used to reduce the strength of interaction caused by cross coupling in the system. Hence, this work builds the basis for further analysis including the FAIR beam phase control loop, which acts on reference signals [12] and does not change the average RF frequency.

Acknowledgments

We would like to thank all colleagues of the Ring RF Department at GSI for the good collaboration and many fruitful discussions.

References

[1] Robinson K W 1956 *Radiofrequency Acceleration II* (Massachusetts: Cambridge Electron Accelerator)
[2] Pedersen F 1975 Beam loading effects in the cern ps booster *IEEE Trans. Nuc. Sci.* **22** 1906-9
[3] Boussard D 1985 Control of cavities with high beam loading *IEEE Trans. Nuc. Sci.* **32** 1852-6
[4] Koscielniak S R 1993 *Proc. of Int. Conf. on Particle Accelerators 1993 (Washington, DC)* vol 5 (New York: IEEE) pp 3506-8
[5] Lens D, Hülsmann P and Klingbeil H 2009 *Proc. of Particle Accelerator Conf. 2009 (Vancouver): Beam Loading Effects on the RF Control Loops of a Double-Harmonic Cavity System for FAIR* pp 2249-51
[6] Gross K, Klingbeil H and Lens D 2014 *Proc. of the Int. Particle Accelerator Conf. 2014 (Dresden): Impact of Simplified Stationary Cavity Beam Loading on the Longitudinal Feedback System for SIS100* vol 5 (Geneva: JACoW Publishing) pp 1736-8
[7] Mihailescu-Stoica D, Domont-Yankulova D, Lens D and Klingbeil H *Proc. of the Int. Particle Accelerator Conf. 2018 (Vancouver): Cavity Impedance Reduction Strategies during Multi Cavity Operation in the SIS100 High Intensity Hadron Synchrotron* vol 9 (Geneva: JACoW Publishing) pp 4863-5
[8] Koenig H G et al. 2018 *Proc. of the Int. Particle Accelerator Conf. 2018 (Vancouver): The FAIR-SIS100 Accelerating RF Station* vol 9 (Geneva: JACoW Publishing) pp 2762-4
[9] Schmidt J S, Balß R, Frey M, Hülsmann P, Klingbeil H, König H G, Laier U, Lens D E M and Stuhl A 2018 *Proc. of the Int. Particle Accelerator Conf. 2020 (Caen): The SIS100 RF Systems - Updates and Recent Progress* vol 11 (Geneva: JACoW Publishing) pp 26-30
[10] Klingbeil H, Laier U and Lens D 2015 *Theoretical Foundations of Synchrotron and Storage Ring RF Systems* ed. C Caron et al. (Cham: Springer)
[11] Kronshorst L 2022 *Master Thesis: Measuring and Modeling of an RF Acceleration Cavity* (Darmstadt, Technische Univerität Darmstadt)
[12] Klingbeil H, Laier U, Ningel K P and Schäfer S, Thielmann C and Zipfel B 2011 New digital low-level rf system for heavy-ion synchrotrons *Phys. Rev. ST - Accel. and Beams* **14** 102802
[13] Lens D, Groß K, Klingbeil H, Laier U and Zipfel B 2022 *Heavy-Ion Synchrotron and Storage Ring LLRF Systems at GSI and FAIR: Status and Machine Development Experiment Results* (Brugg-Windisch: LLRF Workshop 2022)
[14] Lunze J 2014 *Regelungstechnik 2: Mehrgrößensysteme, Digitale Regelung* vol 8 (Berlin: Springer Vieweg)
[15] Wegmann C J 2022 *Master Thesis: Analysis and Simulation of the Coupled Control Loops of the Future SIS100 Acceleration Cavities* (Darmstadt, Technische Univerität Darmstadt)